

Microdiffraction from Antiphase Domain Boundaries in Cu_3Au

BY JING ZHU* AND J. M. COWLEY

Department of Physics, Arizona State University, Tempe, Arizona 85287, USA

(Received 15 February 1982; accepted 5 May 1982)

Abstract

Electron diffraction patterns have been obtained from regions of a thin crystal of partially ordered copper-gold alloy, Cu_3Au , which have a diameter of about 15 Å and contain an antiphase domain boundary. The superlattice diffraction spots show a characteristic splitting similar to the splitting which appears in all spots, both fundamental and superlattice, when the beam irradiates a region at the edge of a crystal. By observing which of the superlattice spots are split and which are not, it is possible to deduce immediately whether the antiphase domain boundary is of the 'good' type or is one of the 'bad' types or whether more than one boundary is illuminated by the beam. The observations of split spots are in good agreement with the results of calculations made on the basis of kinematic theory. It is shown that these results remain valid in the presence of strong dynamical scattering for small specimen thicknesses.

1. Introduction

It has been known for many years that in partially ordered alloys such as Cu_3Au small domains of the ordered structure are present, separated by antiphase domain boundaries (APBs). The form of the domain gives characteristic shapes to the superlattice reflections. When the APBs appear at regularly spaced intervals the superlattice spots are split into characteristic doublets or more complicated groupings, having separations inversely proportional to the domain boundary periodicity (Raether, 1952; Yamaguchi, Watanabe & Ogawa, 1962). The existence of antiphase boundaries has also been inferred from electron micrographs which show lattice fringes having the periodicity of the ordered Cu_3Au lattice planes (Sinclair & Thomas, 1975).

It has been recognized (Yamaguchi, Watanabe & Ogawa, 1962) that the antiphase boundaries in Cu_3Au may be of several different types depending on the translation vector which defines the relative positions of

the Au atoms in the adjacent domains. If the translation vector is parallel to the plane of the domain boundary, which is assumed to be parallel to the (100)-type lattice planes, the boundary is of the 'good' type, so called because the nearest-neighbor coordination of the Au and Cu atoms remains unchanged at the boundary. If the translation vector is not parallel to the boundary plane, the boundary introduces changes in the nearest-neighbor coordinations and the boundary is said to be of a 'bad' type.

Some conclusions have been drawn from diffraction evidence concerning the relative numbers of good and bad domain boundaries (Moss, 1964) but direct evidence concerning their existence is lacking.

We have now shown that evidence concerning the nature of individual APBs can be derived from electron diffraction patterns taken from specimen regions of about 15 Å diameter. Patterns of this sort are produced in a scanning transmission electron microscope when the incident electron beam is held stationary on the specimen (Cowley, 1981*a*). When the incident electron beam comes from a very small bright source, the electron wave striking the specimen is highly coherent and a number of striking interference effects are produced (Cowley, 1979*a*). Of particular relevance for our present purposes is the observation that when the incident electron beam is close to the edge of a crystal the diffraction spots show a fine structure, usually in the form of a splitting into two components separated by a distance approximately equal to the diameter of the diffraction spots given by a perfect thin crystal (Cowley & Spence, 1981). This splitting does not reflect any periodicity in the sample. Rather it may be regarded as an interference effect somewhat related to Fresnel diffraction in that it involves the relative phases and amplitudes of the wave functions of the electron wave passing through the edge of the specimen and those passing outside the specimen.

It is to be expected that any discontinuity in the crystal structure such as a crystal defect may also give rise to a splitting of the spots. An isolated antiphase domain boundary is a case in point. Since a discontinuity is present in the superlattice, some splitting of the superlattice diffraction spots should appear. It must be emphasized that this splitting is completely independent of any splitting which may appear in sharply

* On leave from Central Iron and Steel Research Institute, Beijing, The People's Republic of China.

focused diffraction patterns, resulting from periodic repetition of APBs. We are concerned with the splitting of spots produced by a single APB which is illuminated by an electron beam of diameter much smaller than the periodicity of the long-period structures.

The form of the splitting to be expected is derived by use of a simple theoretical treatment. In order to demonstrate the effect, we have used specimens having well-defined APBs, sufficiently well separated to avoid too much confusion from overlapping in the thin films used. These were samples annealed at a temperature below the critical temperature for sufficient time to allow the domains to form and grow to dimensions comparable with the film thickness.

2. The basic theory

In order to establish the nature of the diffraction effects to be observed when a narrow beam of electrons illuminates an antiphase boundary, we make use of the weak-phase-object approximation, *i.e.* we assume that the diffraction amplitudes outside the zero beam are given by the Fourier transform of the projection of the crystal structure in the beam direction. This approximation involves the assumption that the phase change of the electron wave passing through the thin-film sample is small. For copper-gold alloys this assumption is poor for films which are only 20–30 Å thick, which is much thinner than the films which can be conveniently prepared experimentally (Cowley & Murray, 1968). However, arguments will be made that the results of this kinematical treatment can be applied, when suitably modified, to describe the general features, although not the exact intensities, of the diffraction from films of thickness up to 100 Å or more.

The Cu_3Au lattice, viewed in the $[100]$ direction, may be represented as in Fig. 1(a). The four sites per unit cell are designated as $a(0,0)$, $b(\frac{1}{2},0)$, $c(\frac{1}{2},\frac{1}{2})$ and

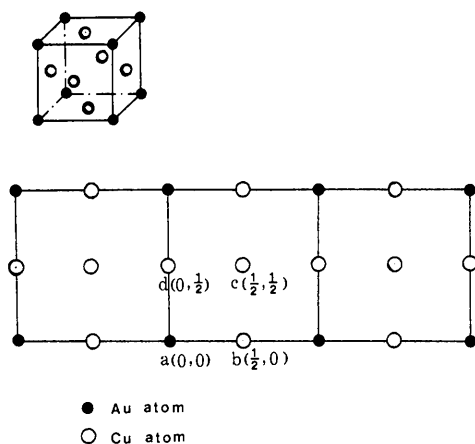


Fig. 1. The Cu_3Au structure, viewed in the $[100]$ direction.

$d(0,\frac{1}{2})$ where the bracketed figures indicate the two-dimensional fractional coordinates. For a 'good' antiphase boundary, at which the nearest-neighbor coordination of the atoms remains unchanged, the Au atoms shift from site a to site d as in Fig. 2(a). 'Bad' antiphase boundaries at which the nearest-neighbor coordination is changed are given by shifts from a to b or from a to c as in Figs. 2(b) and (c).

The superlattice reflections from partially ordered structures or the diffuse scattering from disordered structures are given by the deviation from the periodic average structure (for a review, see Cowley, 1981b). For kinematical electron scattering the relevant scattering functions are then $\frac{3}{4}[\varphi_{\text{Au}}(r) - \varphi_{\text{Cu}}(r)]$ at an Au atom site and $-\frac{1}{4}[\varphi_{\text{Au}}(r) - \varphi_{\text{Cu}}(r)]$ at a Cu atom site where $\varphi_{\text{Au}}(r)$ is the projected potential distribution for an Au atom. For convenience we designate these functions as $3\Delta\varphi$ and $-\Delta\varphi$ respectively and their Fourier transforms as $3\Delta f$ and $-\Delta f$.

The kinematical electron diffraction amplitudes from a very thin crystal film are given by the Fourier transform of the two-dimensional function representing the projection of the potential in the incident-beam direction.

For an ordered Cu_3Au structure the projected potential is made up of the projected potential

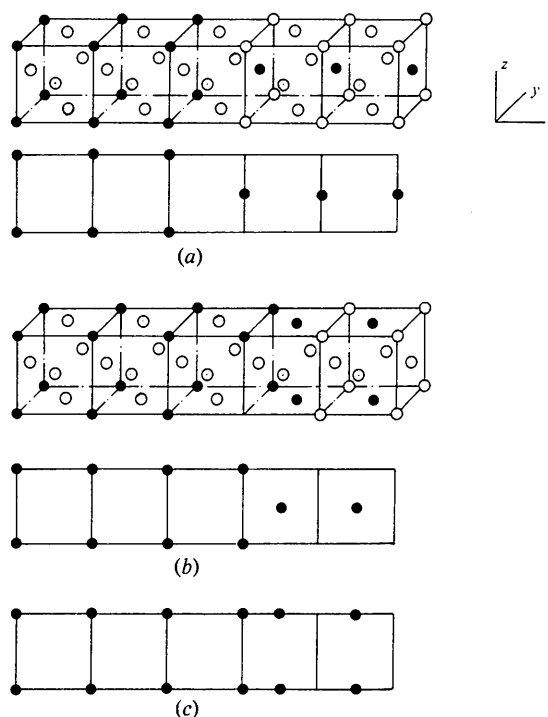


Fig. 2. The types of boundaries for Cu_3Au . (a) A 'good' boundary and the projection of the lattice (Au atom only); (b) a 'bad' boundary and the projection of the lattice from the z -direction, 'bad 1' (Au atom only); (c) a 'bad' boundary and the projection of the lattice from the y direction, 'bad 2' (Au atom only).

distribution of a gold atom at (0,0) and that of a copper atom at $(\frac{1}{2}, 0)$, $(\frac{1}{2}, \frac{1}{2})$ and $(0, \frac{1}{2})$, as suggested by Fig. 1. The deviation of the projected potential from that of the average structure is then

$$\begin{aligned} \varphi(xy) = \Delta\varphi(xy) * [3\delta(xy) - \delta(x - \frac{1}{2}, y) \\ - \delta(x - \frac{1}{2}, y - \frac{1}{2}) - \delta(x, y - \frac{1}{2})] \\ * \sum_n \sum_m \delta(x - n, y - m), \end{aligned} \quad (1)$$

where the * sign represents a convolution operation. The diffraction amplitudes then are given by Fourier transform of (1) as

$$\begin{aligned} \Phi(u, v) = \Delta f [3 - \exp(\pi i h) - \exp\{\pi i(h + k)\} \\ - \exp(\pi i k)] \sum_h \sum_k \delta(u - h, v - k) \\ = \begin{cases} 0 & \text{for } h, k \text{ even} \\ 4 & \text{otherwise,} \end{cases} \end{aligned} \quad (2)$$

i.e. there is diffracted intensity at the superlattice reflection positions due to the ordered deviations from the average structure. If the structure is illuminated by an incident beam of finite diameter instead of by a plane wave, we assume an incident amplitude distribution having the form $b(x, y)$, which multiplies the transmission function of the sample, proportional to the projected potential. The diffraction amplitude will then be spread by convolution with $B(u, v)$, the Fourier transform of $b(xy)$.

For a good antiphase boundary, Fig. 2(a), the projected potential shows a positive deviation from the average potential of $+3\Delta\varphi$ at the gold atom positions (0,0) on one side of the boundary. On the other side of the boundary the positive deviation, $+3\Delta\varphi$, is at $(0, \frac{1}{2})$, the *d* site in Fig. 1. Hence at the boundary the occupancy of the *a* site of Fig. 1 changes from $+3\Delta\varphi$ to $-\Delta\varphi$ and the occupancy of the *d* site changes in the reverse way. We represent these changes by multiplying these deviations from the average projected structure by

$$s(x) = \begin{cases} -1 & \text{for } x < 0 \\ +1 & \text{for } x > 0. \end{cases}$$

The deviation of the projected potential from that of the average structure is then given by

$$\begin{aligned} \varphi(xy) = \left\{ \Delta\varphi(xy) * \sum_{n,m} \delta(x - n, y - m) \right. \\ * \{ \delta(x, y) + \delta(x, y - \frac{1}{2}) - \delta(x - \frac{1}{2}, y) \\ - \delta(x - \frac{1}{2}, y - \frac{1}{2}) \} - \Delta\varphi(xy) \\ * 2s(x) \sum_{n,m} \delta(x - n, y - m) * [\delta(xy) \\ \left. - \delta(x, y - \frac{1}{2}) \right] \} b(xy). \end{aligned} \quad (3)$$

The Fourier transform of $s(x)$ is $S(u) = (\pi u i)^{-1}$. Convolution of any function by u^{-1} has the effect, to a first approximation, of producing the differential of the function with respect to x except that the lower-order Fourier coefficients are emphasized relative to the higher-order coefficients. In the Fourier transform of (3), $S(u)$ is multiplied by $\Delta f(u, v)$ which is a slowly varying function of u , so that we may write

$$\{S(u) \Delta f(u, v)\} * B(u, v) \approx iCB'(uv), \quad (4)$$

where C is a constant and the prime indicates differentiation of B with respect to the u coordinate only. If $B(u, v)$ represents the transmission function of an objective aperture used to define a convergent beam incident on the specimen, the form of $B'(u, v)$ will be as suggested in Fig. 3. In one dimension, differentiation and squaring of the top-hat function $B(u)$ gives two sharp peaks. These will be spread out by the emphasis of the lower-order Fourier coefficients to give $B'^2(u)$. A similar procedure applied to the two-dimensional aperture function $B(u, v)$ gives the two arcs of the final diagram of Fig. 3.

The diffraction amplitude derived from (3) is then

$$\begin{aligned} \Phi(u, v) = \Delta f [1 \pm \exp(\pi i k) - \exp(\pi i h) \\ - \exp\{\pi i(h + k)\}] \sum_{hk} \delta(u - h, v - k) \\ * B(uv) - 2iC\Delta f [1 - \exp(\pi i k)] \\ \times \sum_{h,k} \delta(u - h, v - k) * B'(uv). \end{aligned} \quad (5)$$

Hence the intensity distribution round the superlattice points takes the form $B^2(u, v)$ at (1,0) and $B'^2(u, v)$ at (0,1) and (1,1) as suggested in Table 1.

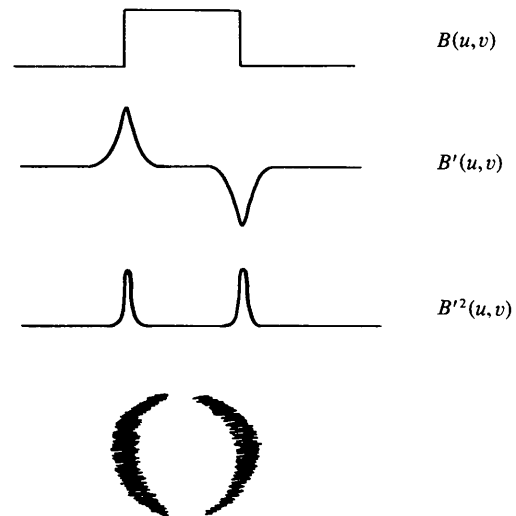
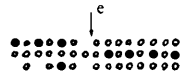
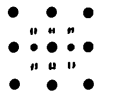
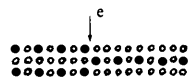
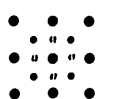
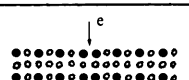
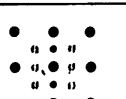
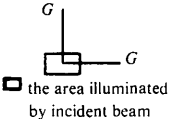
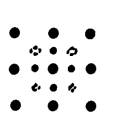
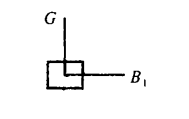
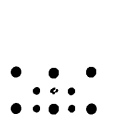
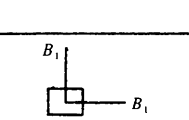
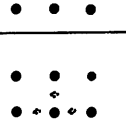
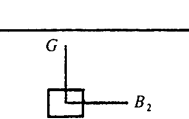
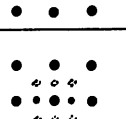


Fig. 3. The form of $B'(u, v)$ for a circular objective aperture.

Table 1. *The form of the splittings of diffraction spots for various combinations of antiphase boundaries*

Type	Name	Boundary case	Diffraction pattern
Single	'Good' boundary G		
	'Bad' boundary B_1		
	'Bad' boundary B_2		
Double	'Good' and 'good', 'Bad' and 'bad' ₂		
	'Good' and 'bad'1 or 'Bad' and 'bad'1		
	'Bad' and 'bad'2		
	'Good' and 'bad'2		

In the same way we can deduce that for a 'bad' domain boundary with a shift from site a to site b the (0,1) spots will be unsplit and the (1,0) and (1,1) spots will be split in the u direction as suggested in Table 1. If the 'bad' domain boundary has a shift from site a to site c , the (1,0) and (0,1) spots will be split and the (1,1) spot will be unsplit, as suggested in Table 1.

It follows from the arguments of Cowley & Fields (1979) that these kinematical results can be used as a guide to the form of the diffraction pattern to be expected from single-crystal films of experimentally accessible thicknesses. These authors showed that, even in the presence of the strong dynamical diffraction effects which are expected for these alloys, the diffraction pattern is given by multiplying the kinematical diffraction intensities by a slowly varying 'dynamical function'. Relative intensities over small reciprocal-space distances will not be strongly modified even though the dynamical scattering by the sublattice

reflections will profoundly influence the relative intensities of points separated by one or more reciprocal-lattice periodicities. Hence we may conclude that the predictions made by our simple theory on the splittings to be observed of the superlattice reflections should correspond to the observations.

More complicated structures arise when the incident beam covers more than one antiphase domain boundary. This may happen when two boundary planes, both parallel to the incident-beam direction, meet near the center of the beam. Also, it is possible that when the domain size is less than the film thickness two domain boundaries may overlap in projection.

For two domain boundaries in the beam the effects on the diffraction pattern will depend on the combination of good and bad boundaries present. In Table 1 we suggest the form of the splittings of diffraction spots to be expected for these various combinations. Some ambiguities are evident in these cases.

3. Experimental procedures

Thin films of Cu_3Au alloy were prepared by vacuum evaporation and epitaxial growth on cleavage surfaces of sodium chloride. Pure Au and Cu metals were evaporated simultaneously. The technique has been described by Ino, Watanabe & Ogawa (1964). However, it may be emphasized that in preparing the cleavage surfaces of the sodium chloride a proper cleaving procedure should be used without applying excessive force. Also, the substrate temperature should be maintained at 673 to 678 K and the pressure should be carefully maintained at 1100 mPa during the evaporation. Estimates based on the quantities evaporated and on X-ray microanalysis of the films suggested the composition to be within 5% of Cu_3Au .

We did not find it necessary to evaporate silver or copper on the cleavage surface [following Pashley & Presland (1958-9) and Hashimoto & Ogawa (1970)] before evaporating the Cu and Au. The film thicknesses used were about 100 Å. After evaporation the samples were heat treated at 603 K for 1-5 h. This temperature is appreciably lower than the critical temperature for ordering, 663 K, so that long-range order was being formed. However, the annealing time was not sufficient to allow the domain size to grow to more than about 50 Å.

Microdiffraction patterns and both dark-field and bright-field electron micrographs were obtained using the HB5 scanning transmission electron microscope from VG Microscopes Ltd, with the attached optical system (Cowley, 1979b) and rapid recording system (Cowley, 1981a). For the microdiffraction an objective aperture size of 10 μm and a focal length of 3 mm gave a beam-convergence angle of 10^{-3} rad so that the beam diameter at the specimen level was about 15 Å. Since

the resolution of the microscope is better than 5 \AA this limitation of the incident-beam convergence is sufficient to ensure that spherical aberration effects are negligible and the diameter of the beam on the specimen is determined by diffraction at the objective aperture only. The diffraction patterns were formed on a fluorescent screen. The light output from the screen was amplified by use of an image intensifier, observed by use of a low-light-level TV camera and recorded on videotape. Photographic records were made from single videotape frames. Mirrors placed in the optical system, between the image intensifier and the TV camera, were used to collect the light from the central spot of the diffraction pattern and produce bright-field images to show the specimen region giving rise to the diffraction patterns. Dark-field images from the superlattice spots only, excluding both the central beam and all the sublattice reflections, were obtained by use of a hollow square aperture of the form illustrated in Fig. 4.

In order to obtain sequences of microdiffraction patterns from systematically chosen specimen regions, the beam was scanned slowly over the specimen (line scan 5 s ; frame time 500 s). With the magnification setting of 10^6 , the beam then scans over a domain of diameter 50 \AA in $1/12.5 \text{ s}$ so that several diffraction patterns could be obtained per domain on the videotape.

High-resolution images of the films were also obtained using a JEM-200CX electron microscope.

4. Results

The high-resolution TEM image, Fig. 5, shows the 4 \AA fringe periodicity of the ordered structure. The out-of-phase domain structure is clearly visible with domain boundaries separated on the average by about 50 \AA .

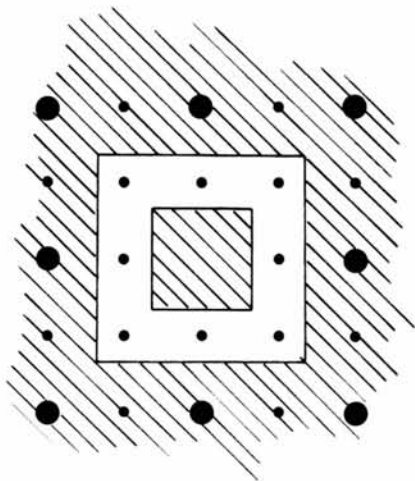


Fig. 4. The hollow square detector aperture is used for dark-field STEM.

Previous observations on similar specimens (*e.g.* Fisher & Marcinkowski, 1961), using diffraction contrast without fringe resolution, have indicated a similar configuration. The domain size is consistent with X-ray diffraction observations of specimens annealed for relatively short periods below the critical temperature.

It is evident that images such as Fig. 5 cannot give information concerning the nature of the antiphase domain boundaries. The orientation and thickness of the film vary over distances of a few hundred \AA . The fringe images cannot be interpreted in terms of atom positions, especially in domain boundary regions, without detailed comparison of the observed images with images computed for precisely defined values for the crystal thickness, the crystal orientation and the lens aberrations, including defocus.

Microdiffraction patterns taken from various regions showed a variety of spot-splitting effects. Fig. 6 shows a pattern in which both the fundamental and superlattice spots are split. This is to be expected when the beam is at the edge of a crystal or at a grain boundary with only one of the grains aligned to give the axial diffraction pattern (Cowley & Spence, 1981). When the beam is entirely within one domain and does not illuminate an antiphase boundary none of the spots show any splitting (Fig. 7). Fig. 8 shows diffraction patterns in which the fundamental reflections are not

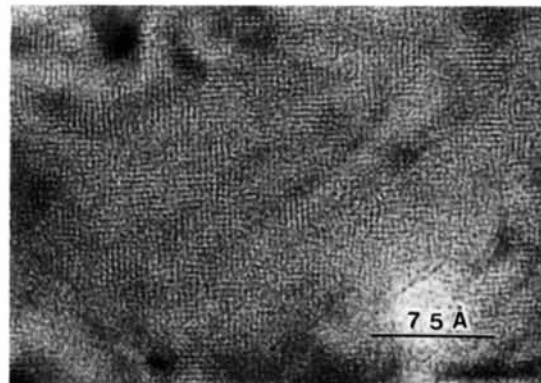


Fig. 5. A high-resolution TEM image showing the 4 \AA fringe periodicity of the ordered structure.

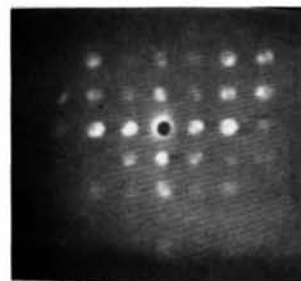


Fig. 6. The diffraction pattern from an edge of a crystal. Both the fundamental and superlattice spots are split.

split but particular groups of superlattice reflections show splittings in accord with the predictions for the various types of APBs. Fig. 8(a) shows the pattern with the two sets of superlattice reflections split but the third set unsplit, as predicted for a good boundary (Fig. 2a). The intensity distribution of the spots is in reasonable agreement with the form suggested by Table 1 with the separation of the two maxima determined by the incident-beam convergence angle defined by the objective-aperture size.

Bright-field and dark-field STEM images of the region giving Fig. 8(b) are shown in Figs. 9(a) and (b). The spot where the beam is stopped to give the microdiffraction pattern is indicated by the small bright rectangular marker. The resolution of the images is necessarily limited by the use of the small objective aperture required to produce the diffraction patterns.

In our experiments most of the microdiffraction patterns were similar to that of Fig. 8(a) in indicating

good boundaries, as suggested in Table 1. Figs. 8(c) and (d) show the splittings characteristic of the two types of bad antiphase boundaries as predicted in Table 1.

For thicker films (300 Å or more) the splitting of the spots was more difficult to observe and usually only a broadening of the spots could be detected. This is consistent with the expectation that for an average domain size of about 50 Å there will usually be five or six domains overlapping in the beam direction and the domain boundaries will either be superimposed or else will be so close together when viewed in the beam direction that characteristic splittings will be confused and the effective decrease of apparent domain size in the projection of the structure will result in a size-effect broadening of the reflections.

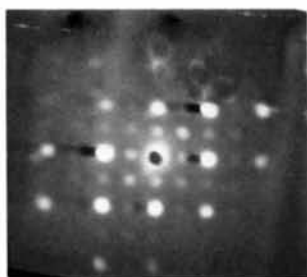


Fig. 7. A diffraction pattern from a region within one domain. The electron beam does not illuminate an antiphase boundary.

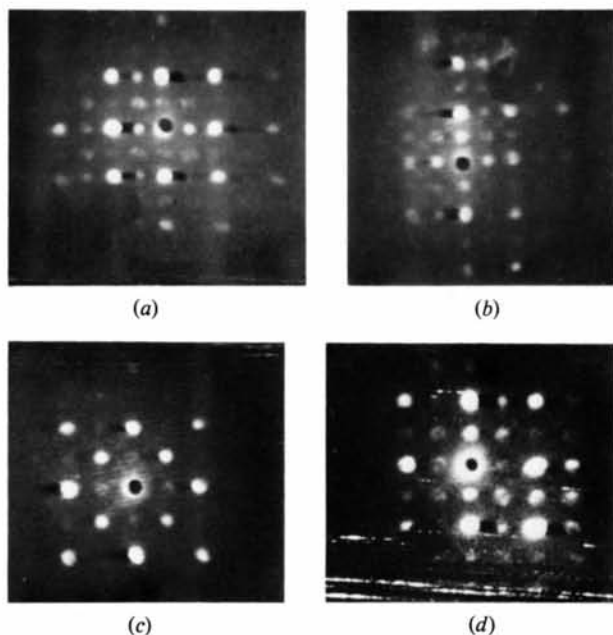
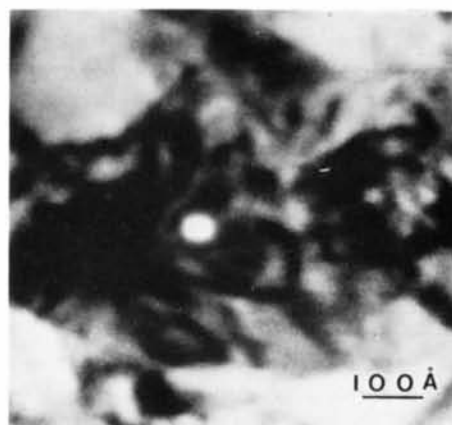
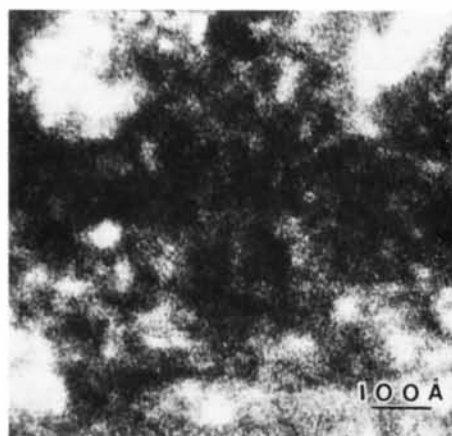


Fig. 8. Diffraction patterns from antiphase boundaries. (a) From a 'good' boundary. (b) From a 'two good' boundary. (c) From a 'bad 1' boundary. (d) From a 'bad 2' boundary.



(a)



(b)

Fig. 9. (a) Bright-field and (b) dark-field STEM images of the region giving fig. 7(b). The small bright rectangular marker indicates the spot where the beam is stopped to give the microdiffraction pattern.

5. Conclusions

It is evident that the use of the microdiffraction technique allows clear deductions to be made concerning the form of the antiphase domain boundaries provided that the single-crystal film is sufficiently thin and the incident beam is of sufficiently small diameter so that there is a relatively low probability that more than one antiphase boundary is illuminated at any time. Given that the orientation of the boundary is indicated by the direction of the spot splitting, the nature of the boundary can be determined unambiguously by observing which spots are split and which are not.

This appears to be the only technique which can be used for this purpose. X-ray diffraction methods can give statistical information in that, on the basis of appropriate assumptions, the relative proportions of good and bad boundaries can be estimated. Computer models of alloys can be generated, consistent with measured values of order parameters, and these can be analyzed in terms of out-of-phase boundary configurations (Gehlen & Cohen, 1965). But these methods become less useful as the degree of order increases. It will not be possible to derive this information directly from high-resolution electron micrographs until such time as it is possible to obtain images from small regions of accurately determined orientation and thickness with a point-to-point resolution approaching 2 Å and then only if careful calculations of intensities are made for precisely determined values of the experimental parameters.

In our case of a Cu_3Au sample with imperfect long-range ordering produced by annealing for a short time at 603 K, it was found that most of the antiphase boundaries were of the good type. Examples of both diffraction patterns of the bad types of boundary could be found occasionally. Fig. 8(c) occurred more frequently than the Fig. 8(d) type.

These results may be used to illustrate the more general contention that microdiffraction may be used in a simple way, without computations, as an aid for the identification of any crystal defect for which the local variation of the symmetry of the structure is such as to affect the amplitudes of some of the diffraction spots but not others. Those reflections which are affected will

show splitting. The detailed interpretation of the intensities of microdiffraction patterns in terms of the atom configurations in defects (Spence, 1978) is, of course, a much more formidable task.

This work was supported by National Science Foundation Grant DMR7926460 and made use of the resources of the Facility for High Resolution Electron Microscopy supported by the NSF Regional Instrumentation Facilities Program, Grant CHE7916098.

References

- COWLEY, J. M. (1979a). *Ultramicroscopy*, **4**, 435–450.
 COWLEY, J. M. (1979b). In *37th Ann. Proc. Electron Microscopy Soc. Am.*, edited by G. W. BAILEY, pp. 379–373. Baton Rouge: Claitor.
 COWLEY, J. M. (1981a). In *39th Ann. Proc. Electron Microscopy Soc. Am.*, edited by G. W. BAILEY, pp. 348–349. Baton Rouge: Claitor.
 COWLEY, J. M. (1981b). *Diffraction Physics*, 2nd ed. Amsterdam: North Holland.
 COWLEY, J. M. & FIELDS, P. N. (1979). *Acta Cryst.* **A35**, 28–37.
 COWLEY, J. M. & MURRAY, P. J. (1968). *Acta Cryst.* **A 24**, 329–336.
 COWLEY, J. M. & SPENCE, J. C. H. (1981). *Ultramicroscopy*, **6**, 359–366.
 FISHER, R. M. & MARCINKOWSKI, M. J. (1961). *Philos. Mag.* **6**, 1385–1405.
 GEHLEN, P. C. & COHEN, J. B. (1965). *Phys. Rev. A*, **139**, 844–855.
 HASHIMOTO, S. & OGAWA, S. (1970). *J. Phys. Soc. Jpn*, **29**, 710–721.
 INO, S., WATANABE, D. & OGAWA, S. (1964). *J. Phys. Soc. Jpn*, **19**, 881–891.
 MOSS, S. C. (1964). *J. Appl. Phys.* **35**, 3547–3553.
 PASHLEY, D. W. & PRESLAND, A. E. B. (1958–9). *J. Inst. Met.* **87**, 419–428.
 RAETHER, H. (1952). *Z. Angew. Phys.* **4**, 53–59.
 SINCLAIR, R. & THOMAS, G. (1975). *J. Appl. Cryst.* **8**, 206–210.
 SPENCE, J. C. H. (1978). In *Electron Microscopy 1978 Vol. 1, Physics*, edited by J. M. STURGESS, pp. 554–555. Toronto: Microscopical Soc. of Canada.
 YAMAGUCHI, S., WATANABE, D. & OGAWA, S. (1962). *J. Phys. Soc. Jpn*, **17**, 1030–1041.